Theor Chim Acta (1987) 71: 359-374

Theoretica Chimica Acta

Application of fixed-nuclei scattering theory to electron methane elastic and inelastic differential cross sections at 10 eV impact energy

Najib Abusalbi, David W. Schwenke, C. Alden Mead, and Donald G. Truhlar

Department of Chemistry, University of Minnesota, Minneapolis, MN 55455, USA

(Received September 24, 1986/Accepted January 28, 1987)

Quantum mechanical calculations are reported for electron-methane elastic scattering and rotational excitation cross sections at 10 eV impact energy. The calculations employ a fixed-nuclei close coupling formalism with full incorporation of symmetry and are used to test previous laboratory-frame calculations employing a direct coupling approximation. Good agreement is obtained. Additional comparisons to previous theoretical and experimental work are also presented, and the contributions of the various symmetries to the cross sections are analyzed in terms of representatve matrix elements of the interaction potential.

Key words: Electron scattering — Close coupling — Elastic scattering — Rotational excitation — Differential cross section

1. Introduction

Two of the authors and coworkers have recently presented a calculation of the elastic scattering and rotational excitation cross sections for electron scattering by ground-state methane [1]. This calculation employed an effective interaction potential including nonadiabatic charge polarization effects and a laboratory-frame close coupling expansion [2, 3] that was converged with respect to the rotational-orbital basis under the direct coupling approximation. In this approximation only channels directly coupled to the initial state by nonzero potential matrix elements are included. Since the validity of this approximation is untested it is desirable to do so, and in the present paper we present a calculation for the same effective potential that is converged without this approximation. Comparison of the cross sections obtained in the two ways provides a test of the direct coupling approximation.

The new calculations reported here are performed by a fixed-nuclei molecule-frame close coupling expansion [4–7] in order to take full advantage of the molecular symmetry. Full details of the molecule-frame formalism are presented in the preceding paper [7]. Although the fixed-nuclei formalism neglects rotational kinetic energy effects that are included in the laboratory-frame calculation, it is widely applied to electron-molecule scattering [8], and the approximation is generally considered not to introduce significant error when the impact energy greatly exceeds the rotational excitation threshold. The latter condition is well satisfied in the present case because the highest final rotational quantum number considered is $j' = 10$, which has an excitation energy of 0.07 eV, whereas the impact energy considered here is a 10 eV. Further discussion of this point is provided in Sect. 4.

Section 2 presents calculational details, Sect. 3 presents the results, and Sect. 4 presents a discussion of these results and a comparison to previous theoretical and experimental work. Section 5 is a brief summary.

2. Calculations

We consider the case of vibrationally and electronically elastic scattering of an electron by CH_4 at 10 eV incident energy. We make the rigid rotator approximation, and we include only one electronic state explicitly in the state expansion. Virtual electronic excitation is included by means of a polarization potential, and in particular we have chosen the effective potential to be the "Static, Exchange, plus local-kinetic-energy-Polarization" (SEPlke) potential used in our previous study [1]. This calculation permits us to test the validity of the direct coupling approximation employed in previous laboratory-frame calculations and the fixed-nuclei approximation employed here by comparing the present cross sections to those of our previous calculation [1].

The SEPlke potential is an *ab initio* one with no adjusted parameters. It has been described in detail in [1] so we only summarize it here. We calculated the static potential, adiabatic polarization potential, and target electronic density from extended-basis-set Hartree–Fock calculations. The exchange potential is evaluated by the semiclassical exchange approximation [9], according to which it is a functional of the static potential and target density. The polarization potential is evaluated by the local-kinetic-energy semiclassical polarization approximation [10] as a functional of the static-exchange and adiabatic polarization potentials. The choice of the SEPlke potential for the previous study gave very good agreement with the most recent experimental differential cross section measurements [11–13].

For electronically elastic scattering the effective potential has the full symmetry of the molecule, and it can be written as [6]

$$v(r, \tilde{\omega}) = \sum_{\lambda=0}^{\infty} \sum_{h_\lambda=1} V_{\lambda h_\lambda}(r) X^{A_1 1}_{h_\lambda \lambda}(\tilde{\omega}) \tag{1}$$

where r is the distance from the center of mass of CH_4 to the electron, $\tilde{\omega}$ denotes angular coordinates $\tilde{\theta}$, $\tilde{\phi}$ with respect to a molecule-fixed frame, $V_{\lambda h_\lambda}$ is an expansion coefficient, and $X^{PU}_{h_\lambda \lambda}$ is a symmetrized harmonic that defines a basis for component U of irreducible representation P of the molecular T_d point group and is defined by

$$X^{PU}_{h_\lambda \lambda}(\tilde{\omega}) = \sum_{m_\lambda} b^{PU}_{h_\lambda \lambda m_\lambda} Y^{m_\lambda}_{\lambda}(\tilde{\omega}) \tag{2}$$

where $b^{PU}_{h_\lambda \lambda m_\lambda}$ is a coefficient and $Y^{m_\lambda}_{\lambda}(\tilde{\omega})$ is a spherical harmonic. Note that Eq. (1) involves only the totally symmetric point group A_1; since this is nondegenerate, $U = 1$. For the present calculations $v(r, \tilde{\omega})$ was expanded in all A_1 symmetrized harmonics with $\lambda \leq 13$. The number of terms in the sum over h_λ is the number of totally symmetric generalized harmonics with λ nodes in $\tilde{\theta}$. Because of the high symmetry of CH_4, there are only 12 terms with $\lambda \leq 13$. Fig. 1 shows the spherical component $V^{\text{Plke}}_{01}(r)$ and the leading nonspherical component $V^{\text{Plke}}_{03}(r)$ of the local-kinetic energy polarization potential and compares them to the spherical components $v_{01}(r)$ of two polarization potentials from the literature, namely the parameter-dependent potential of Gianturco and Thompson [14] (GT) with their empirical cutoff value of $r_0 = 0.88a_0$ chosen by appeal to experimental data and with another cutoff value of $0.84a_0$ that they also used, and thirdly the recent parameter-free polarization model of Jain and Thompson [15] (denoted JT). An interesting aspect of the comparisons is that the polarization potentials used by these workers are assumed spherical while ours does not suffer from this restriction; the figure shows, however, that our $\lambda = 3$ component is about an order of magnitude smaller than our $\lambda = 0$ component. At the outer maximum of the $\lambda = 3$ component, though, it is about one-fourth as large as the $\lambda = 0$ one. The present Plke polarization potential is very similar in strength to the JT potential, and both of these potentials are much less attractive than the older GT potential.

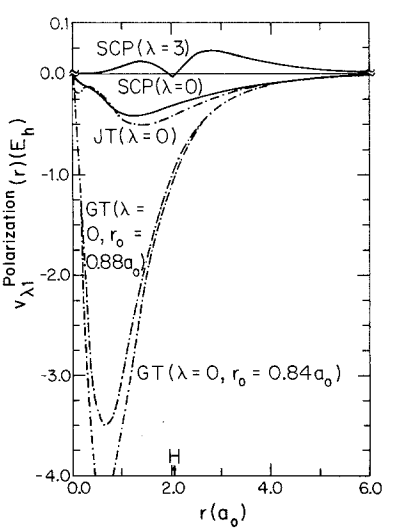

Fig. 1. The $\lambda = 0$ and $\lambda = 3$ components of the Plke polarization potential (in hartrees) as functions of r (in bohrs) are shown as a solid curve. The $\lambda = 0$ components of the polarization potentials of Jain and Thompson (labelled JT) and of Gianturco and Thompson (labelled GT) for the cutoff values $r_0 = 0.88a_0$ and $r_0 = 0.84$ a_0 are shown as dashed curves. Recall that the $\lambda = 0$ components are $(4\pi)^{1/2}$ times the spherical average

The scattering wave function for component U of irreducible representation P is expanded as [6]

$$F^{PU}(\tilde{\boldsymbol{r}}) = \sum_{l=0}^{\infty} \sum_{H=1}^{H_{\max(P,l)}} r^{-1} f_{Hl}^{PU}(r) X_{Hl}^{PU}(\tilde{\omega}) \tag{3}$$

where $\tilde{\boldsymbol{r}}$ denotes $(r, \tilde{\omega})$; f_{Hl}^{PU} is the radial function in channel P, U, H, l; and $H_{\max}(P, l)$ denotes the number of basis functions with the same values of P, U, and l. The resulting close coupling equations are [6]

$$\left[-\frac{\mathrm{d}^2}{\mathrm{d}r^2} + \frac{l(l+1)}{r^2} + \frac{2\mu_r}{\hbar^2} V_{HlHl}^{PU}(r) + \frac{2\mu_r E}{\hbar^2}\right] f_{Hl}^{PU}(r) = -\frac{2\mu_r}{\hbar^2} \sum_{H'l'}' V_{HlH'l'}^{PU}(r) f_{H'l'}^{PU}(r), \tag{4}$$

where μ_r is the reduced mass, $\hbar$ is Planck's constant divided by 2π, $\sum'$ denotes that the sum does not include the term with $H' = H$ and $l' = l$, and

$$V_{HlH'l'}^{PU}(r) = \int \mathrm{d}\tilde{\omega}\, X_{H'l'}^{P'U'*}(\tilde{\omega}) v(r, \tilde{\omega}) X_{Hl}^{PU}(\tilde{\omega}). \tag{5}$$

The close coupling equations given in (4) were solved using the Minnesota Numerov code [16] (MNN, version 80-10A). We solved a separate set of coupled equations for each of the five irreducible representations of the T_d point group, i.e. A_1, A_2, E, T_1, and T_2. The integration was started at $r_0 = 10^{-5}\mathrm{a}_0$ for the A_1 symmetry, which has an $l = 0$ term, and at $r_0 = 10^{-4}\mathrm{a}_0$ for A_2, E, T_1, and T_2, for which min $l \geq 1$. The first four integration steps were carried out with a stepsize of $5 \times 10^{-5}\mathrm{a}_0$, then the stepsize was allowed to grow according to the variable-stepsize algorithm with the parameter DELTA [16] set equal to -1.5×10^{-8}. The stepsize was not allowed to exceed $0.1024\mathrm{a}_0$ in order to avoid numerical instability for r between 30 and $50\mathrm{a}_0$. The ending point at which the molecule-frame T matrix was computed was fixed at $r_{\max} = 50.0\mathrm{a}_0$. This value was chosen such that the dominant reactance matrix elements as well as the eigenphase sum were both converged to 1% or better with respect to increasing $r_{\max}$.

In practice of course the sum over 1 is truncated at a finite number of terms. In order to illustrate the overall degree of convergence with respect to the maximum value of the orbital quantum number retained in the expansion of the scattering function, $l_{\max}(P)$, and consequently the number of channels $N(P)$, results will be presented for two different bases referred to as IV and V. The $N(P)$ and $l_{\max}(P)$ values as well as the eigenphase sums are given for these bases in Table 1. The criterion for basis V was that the dominant T matrix elements are converged to better than 1% while less important ones are reasonably converged. We also include in Table 1 the central-processing-unit (CPU) time for each solution of the coupled equations.

The molecule-frame transition matrices were transformed to the laboratory frame using equations published elsewhere. Basis IV yields laboratory frame results for total angular momentum $J \leq 10$ and basis V yields results for $J \leq 12$. (For larger

Table 1. Basis sets for scattering in the molecule-fixed frame

l_{max}	P	$N(P)$	Eigen phase sum (mod π)	CPU time[a] (min)
10[b]	A_1	8	2.206	2.5
	A_2	3	0.0176	0.9
	E	10	0.7313	3.1
	T_1	12	0.2626	4.5
	T_2	18	0.9546	15.3
	Total			26.3[c]
12[d]	A_1	11	2.212	5.3
	A_2	4	0.0191	1.0
	E	14	0.7386	7.6
	T_1	18	0.2730	14.5
	T_2	24	0.9696	39.3
	Total			67.7[c]

[a] Central processing unit time on the University of Minnesota Department of Chemistry Digital Equipment Corporation VAX 11/780 computer with floating-point accelerator. All calculations were performed in double precision, i.e. with 8-byte words
[b] Basis IV
[c] Total CPU time in minutes
[d] Basis V

J we used the polarized Born approximation [17] to converge the elastic scattering.) The maximum rotational quantum number, $j_{max}(J)$, and a number of channels, $N(J)$, for each J are summarized in Table 2.

A rough idea of the savings in computer time achieved by using the fixed-nuclei formulation of the scattering problem instead of the laboratory-frame formulation including the rotational Hamiltonian can be gained by comparising the basis-V CPU time in Table 1 to the time for a comparable laboratory-frame calculation involving coupled channels solutions for $J \leq 12$ and the polarized Born approximation for $J = 13$–40. Using basis I[1] for $J \leq 12$ shows that the molecule-frame calculation is less CPU-time-consuming by about a factor of two.

3. Results

The first few first-row T matrix elements for $J = 0$ and 1 computed directly in the laboratory-fixed frame and computed by transforming the molecule-fixed T matrix, are listed in Table 3. This table shows excellent agreement of the two independent calculations, confirming the consistency of our equations and our numerical work, and also indicating that the CPU-time savings of the molecule-fixed calculation are achieved with negligible, if any, loss of accuracy.

The convergence of the close coupling bases IV and V is shown in Table 4 where the state-to-state, rotationally elastic and inelastic, and vibrationally elastic, rotationally summed, differential cross sections are listed for selected scattering angles, and in Table 5 where the corresponding integral and momentum transfer

Table 2. Maximum rotational quantum numbers and numbers of channels for each total angular momentum for e^--CH_4 scattering in the laboratory-fixed frame obtained by transforming the molecule-frame transition matrix

Basis	IV[a,b]		V[a,c]	
J	$j_{max}(J)$	$N(J)$	$j_{max}(J)$	$N(J)$
0	10	8	12	11
1	11	15	12	19
2	11	21	12	28
3	11	27	11	31
4	11	31	11	36
5	11	34	11	40
6	10	34	10	39
7	9	30	9	35
8	8	24	8	29
9	8	21	8	26
10	7	13	7	18
11	0[d]	(1)	6	11
12	0[d]	(1)	6	10
13–40	0[d]	(1)	0[d]	(1)

[a] There is no limit on the centrifugal sudden decoupling index n, as used in [12], but all elements with $l > l_{max}$ were zeroed
[b] $l_{max} = 10$
[c] $l_{max} = 12$
[d] Polarized Born T_{11} matrix element

Table 3. A few first row transition matrix elements from $j=0$, $l=J$ to $j' \geq 0$, $|J-j'| \leq l' \leq J+j'$ computed with the SEPlke potential

	$J=0$		$J=1$	
j'	Laboratory[a]	Body[b]	Laboratory[a]	Body[b]
0	(−1.7554, −0.57995)	(−1.7555, −0.57981)	(−0.63358, −0.92919)	(−0.63342, 0.92914)
3	(0.25406, −0.16166)	(−0.25411, −0.16177)	(0.01114, −0.00695)	(−0.01027. 0.00577)
			(0.02080, 0.03509)	(−0.02085, −0.03512)
4	(0.03878, 0.02816)	(−0.03884, −0.02821)	−0.00778, −0.02042)	(0.00794, 0.02025)
			(0.00262, 0.00471)	(−0.00263, −0.00472)
6	(−0.00083, −0.00128)	(0.00084, 0.00129)	(0.00048, 0.00106	(−0.00049, −0.00106)
			(−0.00004, −0.00015)	(0.00004, 0.00015)
7	(0.00006, 0.00017)	(0.00006, 0.00017)	(−0.000001, −0.00013)	(−0.000001, −0.00013)
			(−0.000004, 0.000006)	(−0.000004, 0.000006)

[a] Computed directly in the laboratory-fixed frame using basis I of Ref. [20]
[b] Computed in the molecule-fixed frame, then transformed to the laboratory-fixed frame using basis V

Table 4. State-to-state and vibrationally elastic differential cross sections (a_0^2/sr) at selected angles, computed with laboratory-fixed T matrix elements obtained by transforming the molecule-fixed T matrix

θ (deg)	Basis	$d\sigma_{0j'}/d\Omega$ $j'=0$	3	4	6	7	0-10[a]
0	IV[b]	5.25 (+1)	0	6.09 (−1)	1.62 (−3)	0	5.32 (+1)
	V[c]	5.20 (+1)	0	6.16 (−1)	1.64 (−3)	0	5.27 (+1)
	Exp.[d]						—[e]
40	IV	1.24 (+1)	2.76 (−1)	6.03 (−1)	8.14 (−4)	6.59 (−5)	1.33 (+1)
	V	1.24 (+1)	2.74 (−1)	6.09 (−1)	8.61 (−4)	6.79 (−5)	1.33 (+1)
	Exp.						1.08 (+1)
60	IV	4.81	4.06 (−1)	5.86 (−1)	8.24 (−4)	1.00 (−4)	5.81
	V	4.84	4.08 (−1)	5.92 (−1)	8.89 (−4)	1.00 (−4)	5.85
	Exp.						4.89
90	IV	2.34	2.86 (−1)	5.48 (−1)	2.68 (−3)	1.32 (−4)	3.18
	V	2.35	2.87 (−1)	5.54 (−1)	2.81 (−3)	1.34 (−4)	3.20
	Exp.						2.86
120	IV	3.80 (−1)	9.79 (−2)	5.23 (−1)	8.07 (−3)	3.86 (−4)	1.01
	V	3.75 (−1)	9.89 (−2)	5.29 (−1)	8.25 (−3)	3.90 (−4)	1.01
	Exp.						9.28 (−1)
140	IV	5.43	2.46 (−1)	5.38 (−1)	1.29 (−2)	7.43 (−4)	6.22
	V	5.45	2.49 (−1)	5.45 (−1)	1.31 (−2)	7.50 (−4)	6.25
	Exp.						3.61
180	IV	1.86 (+1)	7.23 (−1)	5.94 (−1)	1.82 (−2)	1.25 (−3)	1.99 (+1)
	V	1.86 (+1)	7.31 (−1)	6.01 (−1)	1.84 (−2)	1.27 (−3)	2.00 (+1)
	Exp.						—[e]

[a]This sum over j' is called $d\sigma_0/d\Omega$ in [20]
[b]Corresponds to $l_{max}=10$ in the molecule-fixed frame
[c]Corresponds to $l_{max}=12$ in the molecule-fixed frame
[d]Experimental values of [36]
[e]Unavailable

cross sections are given. In addition, we compare the differential cross sections in Table 4 to the available experimental measurements of Tanaka et al. [12] (the experimental results of Newell et al [13] agree well with the data of Tanaka et al., as reviewed elsewhere [18]), and in Table 5 we compare the integral and momentum transfer cross sections to the corresponding values obtained directly in the space-fixed frame with two different types of potentials, as well as to the available values obtained by calculations by Jain and Thompson [15]. We have already compared the Jain-Thompson polarization potential to ours, and we note here that they also used a different exchange potential, the Hara-free-electron-gas-exchange approximation, as compared to the one used here. In Fig. 2 we compare the present basis-V calculations of the state-to-state $j=0\rightarrow j'=0$, 3, 4 differential cross sections to those of Jain and Thompson.

The molecule-frame results in Table 5 for the sum over all j' are obtained by transforming the molecule-frame T matrix elements to the laboratory frame, computing cross sections, and summing. This quantity can also be computed

Table 5. Integral and momentum transfer state-to-state and vibrationally elastic cross sections (a_0^2)

	Molecule frame[a]		Laboratory frame		
j'	Basis IV	Basis V	Basis III[b]	Basis III[c]	Jain & Thompson[d]
	$\sigma_{0j'}$				
0	8.32 (+1)	8.32 (+1)	8.34 (+1)	5.81 (+1)	7.60 (+1)
3	3.44	3.45	3.44	8.96	1.91
4	7.05	7.13	7.00	1.42 (+1)	3.87
6	6.36 (−2)	6.51 (−2)	6.28 (−2)	1.29 (−1)	—[e]
7	3.62 (−3)	3.65 (−3)	3.43 (−3)	5.65 (−3)	—[e]
3-10[f]	1.06 (+1)	1.06 (+1)	1.05 (+1)	2.33 (+1)	5.84
0-10[f]	9.38 (+1)	9.39 (+1)	9.39 (+1)	8.14 (+1)	8.18 (+1)
	$\sigma^m_{0j'}$				
0	5.67 (+1)	5.66 (+1)	5.68 (+1)	4.48 (+1)	5.29 (+1)
3-10[f]	1.04 (+1)	1.05 (+1)	1.04 (+1)	2.26 (+1)	5.68
0-10[f]	6.71 (+1)	6.72 (+1)	6.72 (+1)	6.74 (+1)	5.85 (+1)

[a]SEPlke potential, present calculations
[b]SEPlke potential, [20]
[c]SEPa potential, [20]
[d][12]
[e]Unavailable
[f]Summed over the range of j' indicated

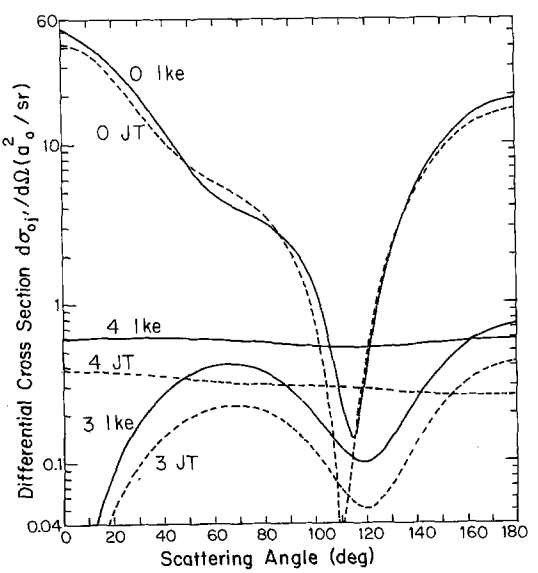

Fig. 2. Differential cross sections for pure elastic scattering (labelled 0 lke JT where lke stands for the semiclassical polarization potential in the local-kinetic-energy approximation, and JT stands for the spherically symmetric polarization potential of Jain and Thompson) and state-to-state rotational excitation cross sections for $j = 0 \rightarrow j' = 3$ and 4 as functions of the scattering angle. The curves labelled lke were calculated with basis V

directly from the molecule-frame T matrix elements by averaging, i.e.

$$\sum_j \sigma_{0j'} = \frac{\pi\hbar^2}{2\mu_r E} \sum_{l'} \sum_{l} \sum_{H'} \sum_{H} \sum_{P} \sum_{U} |T^{PU}_{HlH'l'}|^2 \tag{6}$$

As a further check we calculated this sum from Eq. (6) and obtained complete agreement with the values in the table.

Table 6 presents our full set of state-to-state and vibrationally elastic differential cross sections at 21 scattering angles, while in Table 7 we compute the partial wave contribution q_1 to the integral cross sections obtained with basis V, to the corresponding values computed directly in the laboratory frame with basis III [1] and the SEPlke potential.

Furthermore, in Table 8, we present the individual contributions of the irreducible representations of the T_d point group to the rotational state-to-state and to the rotationally summed integral cross sections. These contributions were obtained by keeping only those molecule-frame T matrix elements corresponding to a particular irreducible representation and nulling those corresponding to the other representations; then transforming to obtain the first row of the laboratory T matrix. Adding the contributions of the various symmetries yields only qualitatively right state-to-state cross sections due to the interference of the different

Table 6. State-to-state, rotationally elastic and inelastic, and vibrationally elastic differential cross sections (a_0^2/sr) at selected angles, using basis V

θ	$d\sigma_{0j'}/d\Omega$					
(deg)	$j'=0$	3	4	6	7	0–10
0	5.20 (+1)	0	6.15 (−1)	1.64 (−3)	0	5.27 (+1)
5	4.76 (+1)	5.69 (−3)	6.16 (−1)	1.59 (−3)	1.25 (−6)	4.82 (+1)
10	4.19 (+1)	2.25 (−2)	6.16 (−1)	1.46 (−3)	4.96 (−6)	4.26 (+1)
15	3.66 (+1)	4.98 (−2)	6.17 (−1)	1.29 (−3)	1.10 (−5)	3.73 (+1)
20	3.11 (+1)	8.68 (−2)	6.17 (−1)	1.13 (−3)	1.95 (−5)	3.18 (+1)
30	2.06 (+1)	1.79 (−1)	6.15 (−1)	9.23 (−4)	4.23 (−5)	2.14 (+1)
40	1.24 (+1)	2.74 (−1)	6.09 (−1)	8.61 (−4)	6.79 (−5)	1.33 (+1)
50	7.30	3.56 (−1)	6.01 (−1)	8.47 (−4)	8.81 (−5)	8.26
60	4.84	4.08 (−1)	5.92 (−1)	8.89 (−4)	1.00 (−4)	5.85
70	3.88	4.12 (−1)	5.80 (−1)	1.16 (−3)	1.08 (−4)	4.88
80	3.23	3.67 (−1)	5.67 (−1)	1.78 (−3)	1.16 (−4)	4.17
90	2.35	2.87 (−1)	5.54 (−1)	2.81 (−3)	1.34 (−4)	3.20
100	1.16	1.94 (−1)	5.41 (−1)	4.28 (−3)	1.79 (−4)	1.90
110	2.50 (−1)	1.22 (−1)	5.32 (−1)	6.12 (−3)	2.63 (−4)	9.11 (−1)
120	3.75 (−1)	9.89 (−2)	5.29 (−1)	8.25 (−3)	3.90 (−4)	1.01
130	2.10	1.41 (−1)	5.32 (−1)	1.06 (−2)	5.57 (−4)	2.79
140	5.45	2.49 (−1)	5.45 (−1)	1.31 (−2)	7.50 (−4)	6.25
150	9.81	4.03 (−1)	5.63 (−1)	1.54 (−2)	9.44 (−4)	1.08 (+1)
160	1.43 (+1)	5.64 (−1)	5.83 (−1)	1.71 (−2)	1.11 (−3)	1.54 (+1)
170	1.75 (+1)	6.86 (−1)	5.96 (−1)	1.80 (−2)	1.22 (−3)	1.88 (+1)
180	1.86 (+1)	7.31 (−1)	6.01 (−1)	1.84 (−2)	1.27 (−3)	2.00 (+1)

Table 7. Partial wave contributions, $q_1(a_0^2)$, to the integral cross sections of Table 6 for the SEPIke potential

l \ j'	0	3	4	6	7	3-10	0-10
0	1.46 (+1)[a]	3.88 (−1)	9.85 (−3)	1.01 (−5)	1.44 (−7)	3.98 (−1)	1.50 (+1)
	1.46 (+1)[b]	3.88 (−1)	9.82 (−3)	9.88 (−6)	1.40 (−7)	3.98 (−1)	1.50 (+1)
1	1.62 (+1)	2.32 (−2)	6.44 (−3)	1.77 (−5)	2.27 (−7)	2.97 (−2)	1.62 (+1)
	1.62 (+1)	2.35 (−2)	6.50 (−3)	1.75 (−5)	2.22 (−7)	3.00 (−2)	1.62 (+1)
2	4.92 (+1)	1.26	6.97	1.31 (−2)	4.38 (−4)	8.24	5.74 (+1)
	4.94 (+1)	1.26	6.85	1.30 (−2)	4.23 (−4)	8.12	5.75 (+1)
3	2.72	1.69	1.13 (−1)	3.80 (−2)	1.38 (−3)	1.84	4.57
	2.73	1.69	1.02 (−1)	3.51 (−2)	1.33(−3)	1.83	4.56
4	3.31 (−1)	7.42 (−2)	3.02 (−2)	1.34 (−2)	1.38 (−3)	1.19 (−1)	4.49 (−1)
	3.32 (−1)	7.28 (−2)	2.92 (−2)	1.45 (−2)	1.27 (−3)	1.18 (−1)	4.50 (−1)
5-8	1.34 (−1)	1.37 (−2)	1.23 (−3)	4.20 (−4)	4.52 (−4)	1.58 (−2)	1.50 (−1)
	1.36 (−1)	1.38 (−2)	1.19 (−3)	9.84 (−5)	4.08 (−4)	1.55 (−2)	1.52 (−1)
9-12	8.79 (−3)	4.01 (−4)	8.0 (−6)	4.9 (−7)	9.6 (−7)	4.02 (−4)	9.20 (−3)
	9.55 (−3)	3.89 (−4)	4.0 (−6)	4.0 (−8)	1.9 (−8)	3.93 (−4)	9.94 (−3)
13-40	8.19 (−3)	0.0	0.0	0.0	0.0	0.0	8.18 (−3)
	2.45 (−3)	9.4 (−5)	0.0	0.0	0.0	9.4 (−5)	2.54 (−3)
0-40	8.32 (+1)	3.45	7.13	6.51 (−2)	3.65 (−3)	1.06 (+1)	9.38 (+1)
	8.34 (+1)	3.44	7.00	6.28 (−2)	3.43 (−3)	1.06 (+1)	9.39 (+1)

[a]Upper entry: molecule frame, basis V
[b]Lower entry: laboratory frame, basis III

representations to reproduce a single T matrix element in the laboratory frame. (Recall that the molecule-frame symmetry classifications are only approximate, as discussed in the previous paper [7]). Finally, in Fig. 3, we plot versus r the first element of the potential matrix for every irreducible representation with and without the centrifugal potential for every symmetry. The terms including the centrifugal potential are defined by

$$W_l^P(r) = V_{1l1l}^{PU}(r) + \frac{l(l+1)}{2r^2}. \tag{7}$$

Table 8. The individual-symmetry contributions $\sigma_{0j'}^{(P)}$ (a_0^2) to the $j \to j' \geq 0$ state-to-state and to the rotationally summed integral cross sections using basis V

P \ j'	0	3	4	6	7	3-10	1-10
A_1	14.8	0.798	0.506	0.308	0.011	1.63	16.4
A_2	0.008	0.000	0.000	0.001	0.000	0.001	0.009
E	4.75	0.002	7.09	0.041	0.001	7.16	11.9
T_1	0.540	0.022	0.073	0.614	0.014	0.779	1.32
T_2	43.3	2.57	18.2	0.199	0.006	21.0	64.3
Vertical Sum	63.4	3.39	25.9	1.16	0.032	30.6	93.9
$\sigma_{0j'}(a_0^2)$	83.2	3.45	7.13	0.065	0.004	10.6	93.9

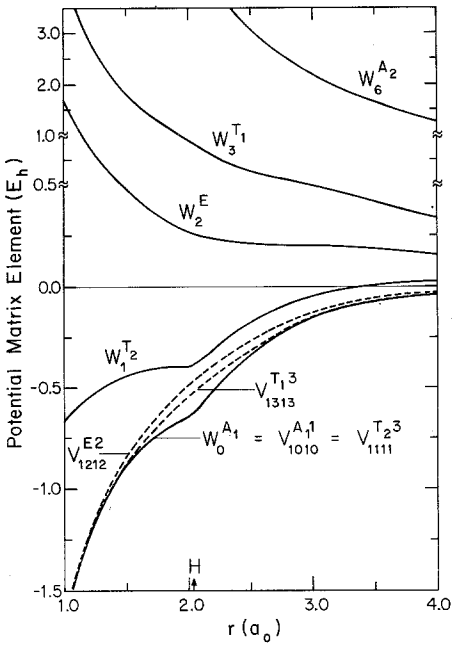

Fig. 3. The first diagonal potential matrix elements (in hartrees) V^{PU}_{1l1l} for each irreducible representation and the corresponding effective potentials W^P_l as functions of r (in bohrs) are shown as solid and dashed curves respectively. Note that $V^{A_2 1}_{1616}$ and V^{E2}_{1212} are indistinguishable on this scale, so only one of them is shown

In Sect. 4 the relative magnitudes of some of the $\sigma^{(P)}_{0j'}$ will be discussed in terms of the centrifugal potentials. We also plot in Fig. 4 two important coupling potential matrix elements for the A_1 representation, namely the $l=3$, $l'=4$ and the $l=3$, $l'=6$ elements, two for the T_2 representation, namely the $l=2$, $l'=3$ and the $l=2$, $l'=4$ elements as well as the diagonal $l=2$, $l'=2$ element for the

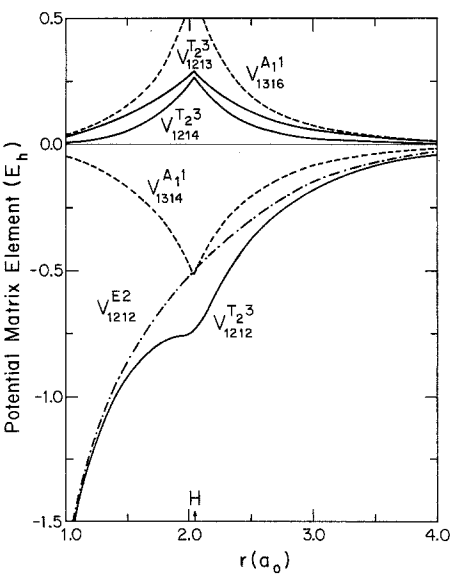

Fig. 4. Some important coupling terms $V^{PU}_{HlH'l'}$ (in hartrees) plotted versus r (in bohrs) for the irreducible representations: T_2, ——; E, — · —; and A_1, - - -

irreducible representations E and T_2. We see from these figures that the regions near the hydrogens dominate the coupling.

4. Discussion and comparison to experiment

Tables 6 and 7 show that the vibrationally elastic, rotationally summed differential, integral, and momentum-transfer cross sections calculated with the T matrix elements obtained by transforming the molecule-fixed frame T matrix to the laboratory-fixed frame, i.e. computed with bases IV and V, are converged to better than 1.5% with the worst relative errors occurring in the differential cross sections for forward scattering angles. The convergence of the state-to-state integral and momentum-transfer cross sections for excitations to $j' \geq 8$ and of the differential cross section for $j' \geq 6$, especially in the forward scattering direction, is not as good, but those poorly converged cross sections are of relatively negligible magnitude. Hence we have not reported any cross sections for $j' \geq 8$.

The degree of agreement of the results obtained in the fixed-nuclei approximation with the results obtained in the laboratory frame, where careful convergence tests have been carried out [1], show that our molecule-frame calculations are well converged. However, we should emphasize that both the molecule-frame and the laboratory-frame calculations compared here contain approximations, in addition to the rigid rotator approximation (neglect of vibration), the approximations in the potential, and the truncations to finite numbers of channels. The molecule-frame calculation reported here is based on the fixed-nuclei approximation, i.e. neglect of the molecular rotational kinetic energy. In principle this assumes $\mu_r / I_A \approx 0$, where I_A is the target's moment of inertia; further discussion of this approximation is given in the introduction. The laboratory-frame formalism presented here does not involve any such additional approximations, but the laboratory-frame calculations reported in [1] involved an additional approximation in the selection of coupled channels, i.e. only channels directly coupled to the ground state by nonzero Hamiltonian matrix elements were included. Ground-state channels have A_1 symmetry in the laboratory frame, and they are coupled directly only to A_1 states with $(-1)^{J+1} = (-1)^J$. However, there are some A_1 channels with $(-1)^{J+l} \neq (-1)^J$ [See Eq. (25b) of [7]]. Although these are not coupled to the ground state, they are coupled to other A_1 states that are coupled to the ground state, and hence they should be included for completeness. The good agreement of the two sets of results in Tables 3 and 5 indicates that neither the fixed-nuclei approximation in the molecule-frame calculations nor the limitation to directly interacting channels in the laboratory-frame ones causes significant errors for these quantities, as well as indicating that both calculations are well converged with respect to including more channels. This provides an important reassurance for future calculations of this type. Quantitatively, Table 5 shows that the relative differences in the state-to-state integral cross sections do not exceed 6% when the column corresponding to basis V is compared to the first of the columns corresponding to basis III of the laboratory frame. Furthermore, Table 7 shows good agreement between the dominant partial-wave contributions to the state-to-state integral cross sections, although it shows larger relative errors

for some higher partial waves which are relatively unimportant or negligible compared to the s, p, d, and f partial waves (and are thus more sensitive to numerical inaccuracies). The effect of neglecting the rotational energy spacings of CH_4 in the present formulation becomes more serious as j' increases, and we find that disagreement with the laboratory frame results becomes more important as j' increases. This trend in the differences is, however, not necessarily due to the fixed-nuclei approximation. Rather it may be due to the difficulty of converging the cross sections for highly excited rotational elvels with respect to the basis set expansion of the wavefunction.

It is clear from Table 5 how sensitive the rotationally elastic and inelastic cross sections are to the type of interaction potential and in particular to the approximations used for polarization. The contribution of the inelastic cross sections to the rotationally summed integral and momentum-transfer cross sections decreases by a factor of 2.2 when we account for non-adiabaticity by using the Plke semiclassical polarization potential instead of the adiabatic polarization potential [1]. It is also interesting to note that the rotationally inelastic cross sections calculated by Jain and Thompson (JT) [15] are even lower than our SEPlke cross sections (by about a factor of 1.8). The dependence upon the type of polarization manifests itself very clearly in the calculations of Gianturco and Thompson (GT) [14] who use a parameter-dependent polarization potential; their differential rotationally summed cross sections, for instance, vary by more than a factor of 2 when they change their empirical parameter (r_0) by only $0.04a_0$. We have also pointed out that we have used the local semiclassical exchange potential, while Jain and Thompson have used the Hara free-electron-gas model exchange potential plus an orthogonalization constraint. It would be interesting to repeat our calculation with a different local exchange model. In Fig. 2 we compare our $0 \rightarrow 0$, $0 \rightarrow 3$, and $0 \rightarrow 4$ differential cross sections to those reported in the recent calculation by Jain and Thompson [15]. Their rotationally elastic cross section shows a much deeper minimum at about 110° compared to ours while their rotationally inelastic $0 \rightarrow 3$ and $0 \rightarrow 4$ cross sections (which are the only two they reported) are consistently lower than ours by about a factor of 2 but are qualitatively similar. We also note that our total integral cross section reported in Table 5, $94a_0^2$, is only about 12% higher than that of Jain and Thompson. The older calculation by Varger et al [19] yields a somewhat higher total integral cross section of $106a_0^2$ at 10 eV, whereas the very recent calculation of Lima et al. [20] yields only $65a_0^2$. Since the primary goals of the new calculations reported here are to test the new symmetry-adapted scattering formalism and to compare molecule-frame and laboratory-frame calculations, we do not discuss these theoretical comparisons in any more detail. We do, however, present next, for completeness, a brief comparison to experiment, and we discuss the contributions of the various molecule-frame symmetries to the calculated cross sections.

The integral elastic and rotationally cross sections are not known experimentally, but the experimental total scattering cross sections provide an upper bound to the 0–10 sum of $\sigma_{0j'}$ shown in Table 5. Furthermore, since the vibrationally and electronically inelastic cross sections are expected to be small at 10 eV, this bound

would be expected to be a close one. An early review [21] of total scattering experiments gave $84a_0^2$ for CH_4 at 10eV and there have been two recent measurements. Barbarito et al [22] obtained $60a_0^2$, and Jones [23] obtained $91a_0^2$. The latter value is encouragingly close to our theoretical value of $94a_0^2$ (Table 5). The fact that the Jones result is the most recent experiment greatly mollifies the otherwise disturbing disagreement with the other recent experiment.

The individual contributions of the irreducible representations to the rotationally summed integral cross sections in Table 8 show that at 10 eV the T_2 representation contributes about 68% of the total cross section, A_1 about 17%, E about 13%, and T_1 and A_2 about 1%. Figure 3 shows that although the $V^{PU}_{H'l'Hl}$ part of the potential is almost indistinguishable (and sometimes actually identical) for some of the individual symmetries, the centrifugal barriers corresponding to $l \geq 6$ prevent most of the scattering effects coming form the A_2 irreducible representation. The large centrifugal barriers for both A_2 and T_1 symmetries explain why all $\sigma^{(P)}_{0j'}$ are small for these P. The T_2 irreducible representation is not only the most important of all for the rotationally summed integral cross sections, it also dominates the contributions of other symmetries to the state-to-state integral cross sections; however these contributions are only qualitative as discussed in the previous section. As an example, we consider the $j=0 \rightarrow j'=3$ cross section. Table 8 shows that the most important symmetry is T_2, while Table 7 shows that the d and f partial waves contribute the most. Hence, the most important coupling terms are the $l=1, l'=2$ and the $l=2, l'=3$ terms. The aboslute difference between the two terms is negligible, hence we chose to plot $V^{T_2 3}_{1213}(r)$ in Fig. 4. Table 8 also shows that the T_2 and the E symmetries are the most important for the $j=0 \rightarrow j'=4$ cross sections; while Table 7 shows that the d wave contributes the most. Hence, the most important coupling terms are the diagonal T_2 and $E_1=2$, $l'=2$ terms and the T_2 off-diagonal $l=2$, $l'=4$ term. These are also plotted in Fig. 4 where we also plot two important A_1 non-diagonal coupling terms, namely $V^{A_1 4}_{1314}(r)$ and $V^{A_1 1}_{1316}(r)$.

The emphasis in this paper is on the convergence of electron-spherical top scattering based on two different formalisms as a test of both. The new calculations are in excellent agreement with previous ones [1], which were compared previously [1] to other results in the literature. Nevertheless, since there have been some new experimental differential cross sections reported since Ref. [1] appeared, we briefly summarize the comparison of theory and experiment for these cross sections. Table 4 shows that our rotationally summed differential cross sections are in good agreement with the experimental measurements of Tanaka et al. [12]. Two more recent experimental measurements [24, 25] of the rotationally summed differential cross sections are compared to those of Tanaka et al. in [25]. Those of Curry et al [24] are in excellent agreement, whereas those of Müller et al. [25] are smaller for $\theta = 80°$–$95°$ and larger for $\theta = 110°$–$140°$. Since our rotationally summed differential cross sections obtained in the present formulation are in excellent agreement with those obtained in our previous laboratory frame formulation [1] and since the previous ones were compared graphically to experimental measurements in [1], we do not repeat the plot against experiment

in the present paper. There is as yet no experiment that resolves the state-to-state rotationally inelastic differential cross sections, although Tanaka et al. [26] and Müller et al. [25] have attempted to analyze the rotationally broadened vibrationally elastic energy loss spectra in terms of individual Δk contributions by a high-j approximation. Müller et al have compared their $j = 0 \rightarrow j' = 0, 3, 4$ results to those of [1] and [15]. The results of [1] are in excellent agreement with experiment for the average magnitude of the cross section in all three cases but for $j' = 0$ and 3, the theoretical results show a deeper minimum than the experimental between 105° and 120°.

5. Summary

Cross sections calculated with a fixed-nuclei electron-molecule scattering formalism are in excellent agreement with previous calculations employing a laboratory-frame approach and a direct coupling approximation. This confirms the essential validity of the fixed-nuclei and direct-coupling approximations and it checks both symmetry-adapted formalisms. Agreement with experiment is also reasonably good, and this confirms the essential validity of the effective potential.

Acknowledgment. This work was supported in part by the National Science Foundation under grant nos. CHE83-17944 and CHE83-11450.

References and notes

1. Abusalbi N, Eades R A, Nam T, Thirumalai D, Dixon DA, Truhlar DG, Dupuis M (1983) J Chem Phys 78:1213
2. Arthurs AM, Dalgarno A (1980) Proc Soc London A 256:540
3. Onda K, Truhlar DG (1978) J Chem Phys 69:1361
4. Temkin A, Vasavada KV (1967) Phys Rev 160:109; Temkin A, Vasavada KV, Chang ES, Silver A (1969) Phys Rev 186:57; Chang ES, Temkin A Phys Rev Lett 23:399
5. Bottcher C (1969) Chem Phys Lett 4:320
6. Burke PG, Sinfailam AL (1970) J Phys B 3:641; Burke PG, Chandra N, Gianturco FA (1972) J Phys B 5:2212
7. Abusalbi N, Schwenke DW, Mead CA, Truhlar DG (1987) Theor Chim Acta 71:333–357
8. See, e.g., the reviews by (a) Lane NF (1980) Rev Mod Phys 52:29 and (b) Burke PG (1980) In: Woolley RG (ed) Quantum dynamics of molecules. Plenum, New York, p 483
9. Riley ME, Truhlar DG (1975) J Chem Phys 63:2182
10. Valone SM, Truhlar DG, Thirumalai D (1982) Phys Rev A25:3003
11. Rohr K (1980) J Phys B 13:4897
12. Tanaka H, Okada T, Boseton L, Suzuki T, Kubo M (1982) J Phys B 15:3305
13. Newell WR, Brewer DFC, Smith AC (1979) XIth International Conference on Electronic and Atomic Collisions, Abstracts (Kytoto), 308
14. Gianturco FA, Thompson DG (1976) J Phys B 9:L383 (1980) 13:673
15. Jain A, Thompson DG (1983) J Phys B16:3077
16. Brandt MA, Truhlar DG, Onda K, Thirumalai D (1980) NRCC Software Catlog, Lawrence Berkeley Laboratory, Berkeley, CA, program No. KQ12. For a discussion of this program see Truhlar DG, Harvey NM, Onda K, Brandt MA (1973) In: Thomas LD (ed) Algorithms and computer codes for atomic and molecular scattering theory, vol. 1, Lawrence Berkeley Laboratory technical report LBL-9501, Berkeley, p 220
17. O'Malley TF, Spruch L, Rosenberg L (1961) J Math Phys 2:491

18. See also Trajmar S, Register DF, Chutjian A (1983) Phys Rep 97:213
19. Varga Z, Gyémánt I, Benedict MG (1979) Acta Univ Szeged 25:85
20. Lima MP, Gibson TL, Huo WM, McKoy V (1985) Phys Rev A32:2696
21. Kieffer LJ (1971) At Data 2:293
22. Barbarito E, Basta M, Calicchio M, Tessari G (1973) J Chem Phys 71:54
23. Jones RK (1985) J Chem Phys 82:5424
24. Curry PJ, Newell WR, Smith ACH (1983) In: Eichler J, Fritsch W, Hertel IV, Stolterfoht N, Wille U (eds) Abstracts of Contributed Papers: Thirteenth International Conference on the Physics of Electronic and Atomic Collisions, Berlin, 1983. North-Holland, Amsterdam, p 244; Curry PJ, Newell WR, Smith ACH (1985) J Phys B 18:2303
25. Müller R, Jung K, Kochem K-H, Sohn W, Ehrhardt H (1985) J Phys B18:3971
26. Tanaka H, Onodera N, Boesten L (1983) In: Eichler J, Fritsch W, Hertel IV, Stolterfoht N, Wille U (eds) Abstracts of Contributed Papers: Thirteenth International Conference on the Physics of Electronic and Atomic Collisions, Berlin, 1983. North-Holland, Amsterdam, p 245